

PAPER • OPEN ACCESS

Numerical modelling of macrosegregation in three-dimensional continuous casting of steel billets

To cite this article: K Mramor *et al* 2023 *IOP Conf. Ser.: Mater. Sci. Eng.* **1281** 012029

View the [article online](#) for updates and enhancements.

You may also like

- [Modelling of macrosegregation in direct chill casting considering columnar-to-equiaxed transition using 3-phase Eulerian approach](#)
J Hao, Y J Lin, Y Nie et al.
- [Prediction of solidification structures in a 9.8 tonne steel ingot](#)
B Gerin, H Combeau, M Založnik et al.
- [Investigation on macrosegregation and dendrite morphology during directional solidification of Al-Cu hypereutectic alloys under a strong magnetic field](#)
Xi Li, DaFan Du, Yves Fautrelle et al.

PRIME
PACIFIC RIM MEETING
ON ELECTROCHEMICAL
AND SOLID STATE SCIENCE

HONOLULU, HI
Oct 6-11, 2024

Abstract submission deadline:
April 12, 2024

Learn more and submit!

Joint Meeting of
The Electrochemical Society
•
The Electrochemical Society of Japan
•
Korea Electrochemical Society

Numerical modelling of macrosegregation in three-dimensional continuous casting of steel billets

K Mramor¹, R Vertnik^{1,2} and B Šarler^{1,3}

¹ Department of Fluid Dynamics and Thermodynamics, Faculty of Mechanical Engineering, University of Ljubljana, Aškerčeva 6, Ljubljana, SI-1000, Slovenia

² Štore Steel d.o.o., Železarska cesta 3, SI-3220 Štore, Slovenia

³ Laboratory for Simulation of Materials and Processes, Institute of Metals and Technology, Lepi pot 11, SI-1000 Ljubljana, Slovenia

* corresponding author: bozidar.sarler@fs.uni-lj.si

Abstract. Macrosegregation presents a considerable defect in the continuous casting of billets and can critically affect the final properties of the product. The numerical modelling can help to predict and better understand the segregation and flow patterns inside the mould. The process is modelled with a physical model described by a set of conservation equations describing the heat transfer, turbulence, fluid flow, solidification and segregation. A two-equation low-Re k -epsilon model and Abe-Kondoh-Nagano closures are used to close governing equations in this incompressible fluid flow example. The Boussinesq approximation is applied to account for the thermo-solutal buoyancy effects, and the Darcy approximation is applied for the description of the flow through the porous mushy zone. On a microscale, a lever rule solidification model is used to couple liquid fraction, temperature and concentration. The three-dimensional model is solved with the method based on local collocation with multiquadric radial basis functions on seven-nodded subdomains. The aim of this contribution is to explore the three-dimensional macrosegregation patterns of 0.51 wt% carbon steel in the solidified shell of the steel in the mould.

1. Introduction

The solidification and macrosegregation of steel in the continuous casting (CC) process is on a macroscale, affected by interconnected complex physical phenomena such as the turbulent motion of molten steel, energy and solute transfer. The consequent variations in the composition, known as macrosegregation, can significantly affect the condition of the product.

The solidification in the CC process, together with the macrosegregation, has been previously extensively studied with a wide variety of numerical methods. The methods considered ranged from classical finite volume [1–6] and finite differences [7] to modern meshless methods [8–11]. In this paper, we apply a local radial basis function collocation method (LRBFCM) [12], for which a three-dimensional (3D) numerical model was constructed to explore the influence of various process parameters on final macrosegregation. The presented model considers the turbulence of incompressible fluid and macrosegregation of 0.51% carbon steel. Among various available turbulence models [13–16], the two-equation low-Re eddy-viscosity model proposed by Abe-Kondoh-Nagano [17] was chosen. This selection is chosen due to its stability and relatively low computational times.



This article explores the effect of input parameters, precisely the casting temperature, velocity, and submerged entry nozzle (SEN) depth, on the final macrosegregation patterns and is a follow-up publication of [9,11].

2. Numerical model

The physical model is posed in the Cartesian coordinate system and formulated within the mixture continuum framework [18], in which steel densities in liquid and solid phases are equal and constant $\rho = \rho_s = \rho_L$. The model describes a simplified 3D CC process and considers the mass

$$\nabla \cdot \mathbf{u} = 0; \quad \mathbf{u} = f_s \mathbf{u}_s + f_L \mathbf{u}_L, \quad (1)$$

momentum

$$\frac{\partial(\rho \mathbf{u})}{\partial t} + \nabla \cdot (\rho \mathbf{u} \mathbf{u}) = -\nabla p + \nabla \cdot [(\mu_L + \mu_t)(\nabla \mathbf{u} + (\nabla \mathbf{u})^T)] - \mathbf{F}_D + \mathbf{F}_B, \quad (2)$$

energy

$$\frac{\partial(\rho h)}{\partial t} + \nabla \cdot (\rho \mathbf{u} h) = \nabla \cdot (\lambda \nabla T) + \nabla \cdot [\rho f_s (h_L - h_s)(\mathbf{u} - \mathbf{u}_s)] + \nabla \cdot (f_L \frac{\mu_t}{Pr_t} \nabla h_L), \quad (3)$$

and species conservation equations

$$\frac{\partial(\rho C)}{\partial t} + \nabla \cdot (\rho C \mathbf{u}) = \nabla \cdot (D \nabla C) + \nabla \cdot [\rho (C_L - C)(\mathbf{u} - \mathbf{u}_s)] + \nabla \cdot (f_L \frac{\mu_t}{\sigma_C} \nabla C_L). \quad (4)$$

The ψ_ℓ ($\psi = \mathbf{u}, C, h, f$) is a general phase variable standing for $\ell = L$ liquid and $\ell = S$ solid phases. The variables used in equations are mixture velocity \mathbf{u} , volume fraction f , time t , pressure p , dynamic viscosity μ_L , turbulent viscosity μ_t , Darcy term $\mathbf{F}_D = \mu_L [(1 - f_L)^2 / (K_0 f_L^3)] (\mathbf{u} - \mathbf{u}_s)$ describing flow through porous media, permeability K_0 , Boussinesq approximation $\mathbf{F}_B = \rho \mathbf{g} [\beta_T (T - T_{ref}) + \beta_C (C_L - C_{ref})]$ describing the effect of the buoyancy on the melt, gravitational acceleration \mathbf{g} , temperature T , reference temperature T_{ref} , thermal expansion coefficient β_T , solute expansion coefficient β_C , the concentration of alloying element C , the nominal concentration of the alloying element C_{ref} , mass-specific mixture enthalpy h , thermal conductivity λ , turbulent Prandtl number Pr_t , diffusivity D , and closure coefficient σ_C . The temperature-enthalpy relation is taken from [18].

The lever rule microsegregation model is given as

$$f_L = 1 - \frac{1}{1 - k_p} \frac{T - T_L}{T - T_m}; \quad C_L = \frac{C}{1 + (1 - f_L)(k_p - 1)}; \quad T_L = T_m + (T_e - T_m) \frac{C}{C_e}, \quad (5)$$

where the partition coefficient is $k_p = C_s / C_L$, T_m are melting and T_e eutectic temperatures, and C_e is eutectic concentration obtained from the iron-carbon phase diagram.

The Low-Re k-epsilon model is used to model the turbulent flow. The equations for turbulent kinetic energy k is defined as

$$\frac{\partial(\rho k)}{\partial t} + \nabla \cdot (\rho \mathbf{u} k) = \nabla \cdot \left[\left(\mu_L + \frac{\mu_t}{\sigma_k} \right) \nabla k \right] + P_k + G_k - \rho \varepsilon + \rho D_k - \mu_L \frac{(1 - f_L)^2}{K_0 f_L^3} k \quad (6)$$

and dissipation rate ε as

$$\frac{\partial(\rho \varepsilon)}{\partial t} + \nabla \cdot (\rho \mathbf{u} \varepsilon) = \nabla \cdot \left[\left(\mu_L + \frac{\mu_t}{\sigma_\varepsilon} \right) \nabla \varepsilon \right] + (c_{1,\varepsilon} f_1 (P_k + c_{3,\varepsilon} G_k) - c_{2,\varepsilon} f_2 \rho \varepsilon) + \rho E - \mu_L \frac{(1 - f_L)^2}{K_0 f_L^3} \varepsilon \quad (7)$$

where σ_k , σ_ε , $c_{1,\varepsilon}$, $c_{2,\varepsilon}$, $c_{3,\varepsilon}$, D_k , E , f_μ , f_1 , and f_2 are Abe-Kondoh-Nagano closures and damping functions [17]. The shear production of turbulent kinetic energy and generation of turbulence due to buoyancy terms P_k and G_k are the same as in [10].

2.1. Numerical implementation

The modern Fortran is used to code the LRBFCM solution. The code is compiled with Intel® Fortran Compiler Classic 2021.7.0 for 64-bit Windows applications. The details of the numerical implementation can be found in [10].

3. Numerical method and solution procedure

3.1. Local radial basis function collocation method

The explicit Euler method is used for time discretisation, and the LRBFCM applied on a local seven-nodded sub-domain is used for space discretisation. The radial basis functions are augmented by a constant, and the shape parameter is set to 32. The incompressibility of the fluid flow is closed by the fractional step method pressure-velocity coupling. A detailed description of the numerical method, its implementation and the solution procedure can be found in [10].

4. Numerical example

4.1. Geometry

The present article's simplified illustration of a CC process is considered as a numerical example. It is represented in simplified 3D geometry and consists of a vertical longitudinal billet of 1.5 m height. The computational domain thickness is set to 0.18 m and accounts for the whole width and depth of the billet. The SEN is set at the top of the billet so that the nozzle entry is 0.12 m below the free surface of the meniscus. Its' inner diameter is 0.035 m and outer diameter is 0.065 m. The height of the mould is 0.8 m. The described geometry was constructed on 473081 nodes and was calculated with time step 10^{-3} s.

4.2. Material Properties

The simplified material properties [19], presented for carbon steel are listed in table 1. In the present model, the carbon content in steel is set to $C_0 = 0.51$ wt%.

Table 1. Material properties and process parameters

	Value	Unit
ρ	7300	kg/m ³
λ	33	W/(m K)
c_{pL}	698	J/(kg K)
c_{pS}	804	J/(kg K)
μ	0.006	kg/(m s)
β_T	10^{-4}	K ⁻¹
β_C	$4.0 \cdot 10^{-3}$	wt% ⁻¹
K_0	10^8	m ²
D_S	$1.6 \cdot 10^{-4}$	m ² /s
D_L	10^{-8}	m ² /s
T_{cast}	1525	°C
T_S	1400	°C
T_L	1482	°C
T_m	1539	°C
u_{cast}	1.6	m/min

4.3. Boundary conditions

The boundary conditions are carefully chosen to solve the problem's strongly coupled governing equations. In the present case, inlet, free surface, moving wall, and outlet boundary condition types are set, as shown in figure 1.

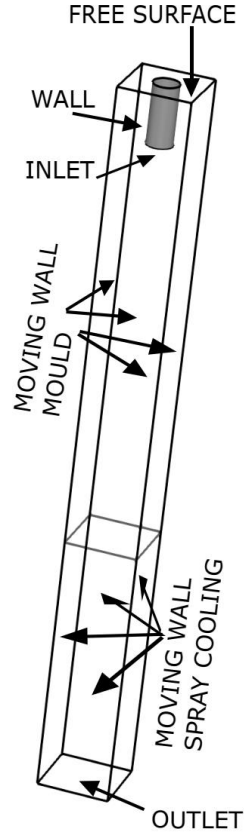


Figure 1. Domain scheme with boundary conditions.

The inlet boundary conditions are prescribed as Dirichlet boundary conditions for temperature $T = T_{\text{cast}}$, velocity $\mathbf{u}(x, y, z) = (0 \text{ m/s}, u_{\text{cast}} 4a_b^2 / (\pi d_2^2), 0 \text{ m/s})$, concentration $C = C_{\text{ref}}$, turbulent kinetic energy $k = 1.5(I_t u_y)^2$; where a semi-empirical correlation for turbulent intensity is calculated as $I_t = 0.16 \text{Re}^{-1/8}$ and $\text{Re} = \rho u_y d_2 / \mu$ is Reynolds number, and dissipation rate $\varepsilon = c_\mu^{0.75} k^{1.5} / (0.07 d_2)$. The Neumann boundary condition is defined for pressure $\partial p / \partial \mathbf{n} = 0 \text{ Pa/m}$. The SEN a_b and billet width d_2 are used for rescaling the casting velocity to maintain a constant flux. The boundary conditions at the free surface are

$$\begin{aligned} \partial u_x / \partial \mathbf{n} = 0 \text{ s}^{-1}; \quad u_y = u_z = 0 \text{ s}^{-1}; \quad \partial T / \partial \mathbf{n} = 0 \text{ K/m}; \quad \partial C / \partial \mathbf{n} = 0 \text{ m}^{-1}; \quad \partial p / \partial \mathbf{n} = 0 \text{ Pa/m}; \\ \partial k / \partial \mathbf{n} = 0 \text{ m/s}^2; \quad \partial \varepsilon / \partial \mathbf{n} = 0 \text{ m/s}^3 \end{aligned} \quad (8)$$

The boundary conditions on the outlet are

$$\begin{aligned} \partial \mathbf{u} / \partial \mathbf{n} = 0 \text{ s}^{-1}; \quad \partial T / \partial \mathbf{n} = 0 \text{ K/m}; \quad \partial C / \partial \mathbf{n} = 0 \text{ m}^{-1}; \quad p = 0 \text{ Pa}; \\ \partial k / \partial \mathbf{n} = 0 \text{ m/s}^2; \quad \partial \varepsilon / \partial \mathbf{n} = 0 \text{ m/s}^3 \end{aligned} \quad (9)$$

The boundary conditions on the moving walls are

$$\begin{aligned} u_x = u_z = 0 \text{ m/s}; \quad u_y = u_{\text{cast}}; \quad q_{cz} = h_{cz}(T - T_{\text{cw}}); \quad \partial C / \partial \mathbf{n} = 0 \text{ m}^{-1}; \quad \partial p / \partial \mathbf{n} = 0 \text{ Pa/m}; \\ k = 0; \quad \varepsilon = 2\mu k_w / (\rho y^2) \end{aligned} \quad (10)$$

The heat flux q_{cz} is calculated as a combination of heat transfer coefficient h_{cz} , which is set to 2000 W/(m² K) at the mould and to 800 W/(m² K) at the secondary cooling system and temperature of the

cooling water T_{cw} set to 293 K. Turbulent kinetic energy is k_w and y is the normal distance to the nearest domain node from the boundary.

5. Results

The concentration fields (C/C_0) are presented for four different casting temperatures at vertical and horizontal cross-sections. The vertical cross-section is shown for an x-y plane in the middle of the billet, and the horizontal cross-section is presented for an x-z plane at the height of 0.19 m. The casting temperatures under observation are 1505°C, 1515°C, 1525°C, and 1535°C. The concentration field is shown in figure 2 and shows that lower casting temperatures result in a more homogeneous concentration field. In general, the concentration in the totally fluid part is close to the nominal concentration. In the mushy region, the concentration is elevated. The most notable differences in the concentration fields can be observed in the totally solid region.

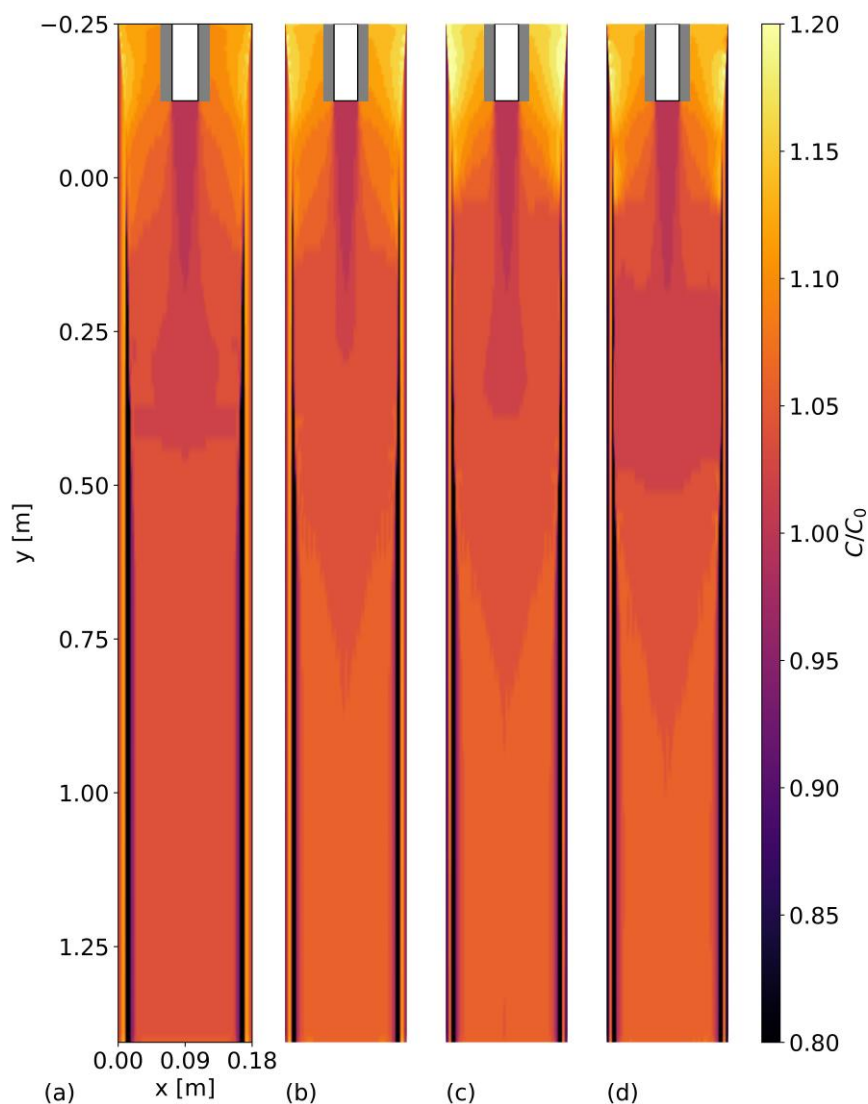


Figure 2. Comparison of concentration fields for different casting temperatures: a) 1505°C, b) 1515°C, c) 1525°C, and d) 1535°C, for a vertical cross-section at the centre of the billet.

Next, the horizontal cross-section placed at $y=0.19$ m is presented in figure 3. Graphs for all temperatures confirm the observation from vertical cross-sections, where the concentration in the totally liquid region at the centre of the billet is close to the nominal concentration. In contrast, the concentration in the mushy zone is depleted. The solidified edges show the most significant difference between the concentration fields.

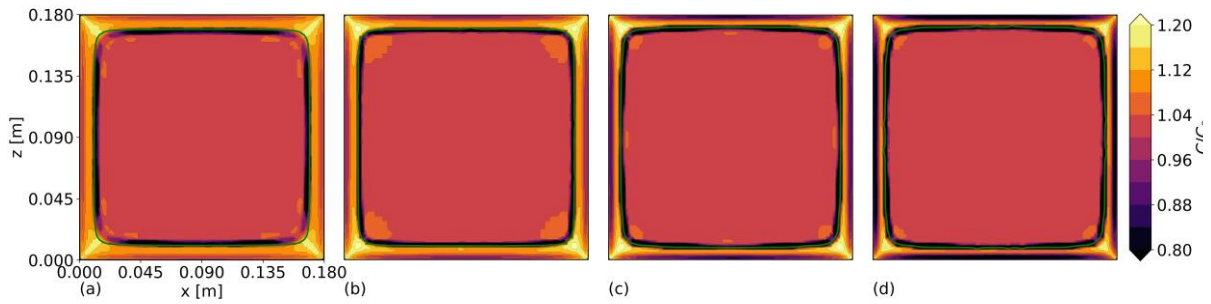


Figure 3. Comparison of concentration fields for different casting temperatures: a) 1505°C, b) 1515°C, c) 1525°C, and d) 1535°C, for a horizontal cross-section at 0.19 m, casting velocity 1.6 m/min and SEN depth 0.12 m. The green line presents a solidus temperature of 1400°C.

The concentration is then compared for different casting temperatures (1505°C, 1515°C, 1525°C, and 1535°C at SEN depth 0.12 m and $u_{cast} = 1.6$ m/min) in figure 4 and for different casting velocities (1.5 m/min, 1.6 m/min and 1.7 m/min at SEN depth 0.12 m and $T_{cast} = 1525$ °C) and different SEN depths (0.10 m, 0.12 m, and 0.13 m at $u_{cast} = 1.6$ m/min and $T_{cast} = 1525$ °C) in figure 5, both at cross-section $y = 0.19$ m and $z = 0.09$ m. The concentration in the liquid is enriched in all of the calculated examples. In the mushy and solid part, the concentration is first depleted, then enriched and again depleted. Higher casting temperatures result in a lower concentration near the boundary.

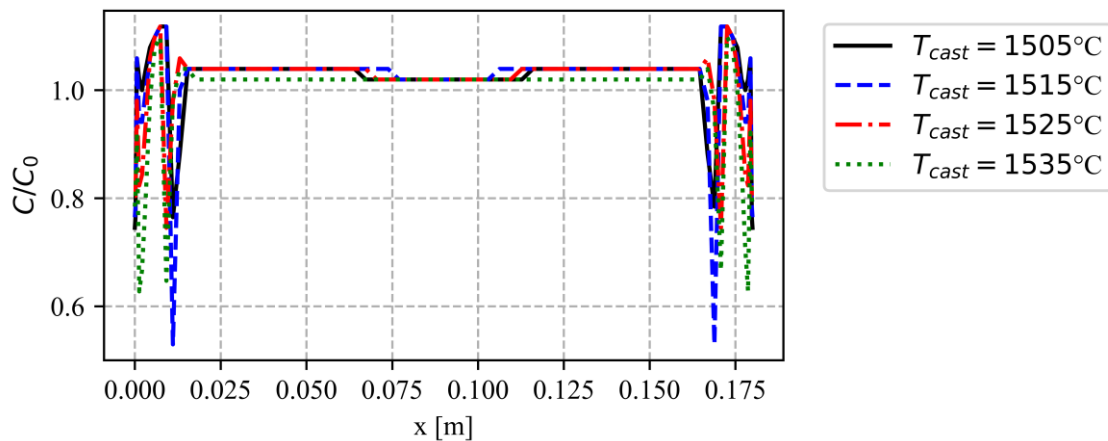


Figure 4. Comparison of concentration cross-sections for different casting temperatures.

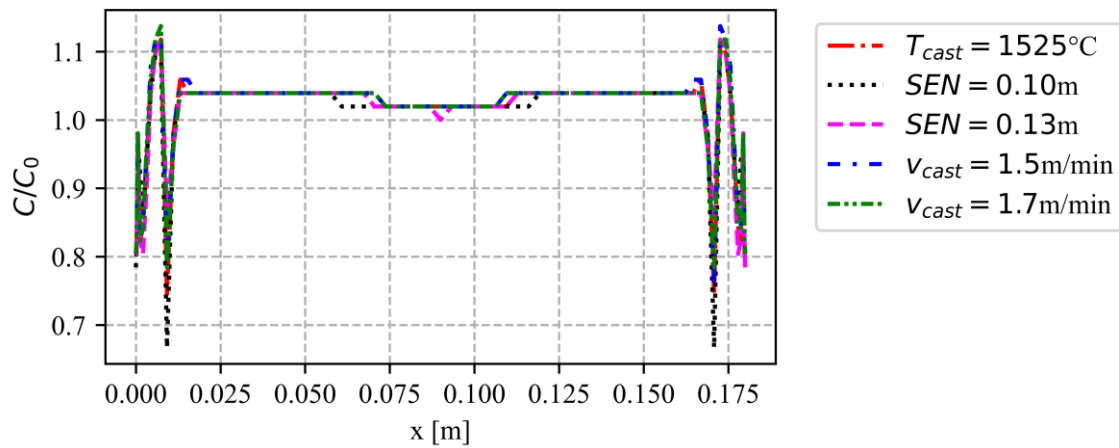


Figure 5. Comparison of concentration cross-sections for different casting velocities and SEN depths.

Figure 6 presents temperature fields at horizontal cross-section $y = 0.19\text{ m}$ for four different casting temperatures. Higher casting temperatures return higher overall temperatures, which is most visible at the centre of the billet. At the boundary, higher temperature gradients result in a higher concentration differences.

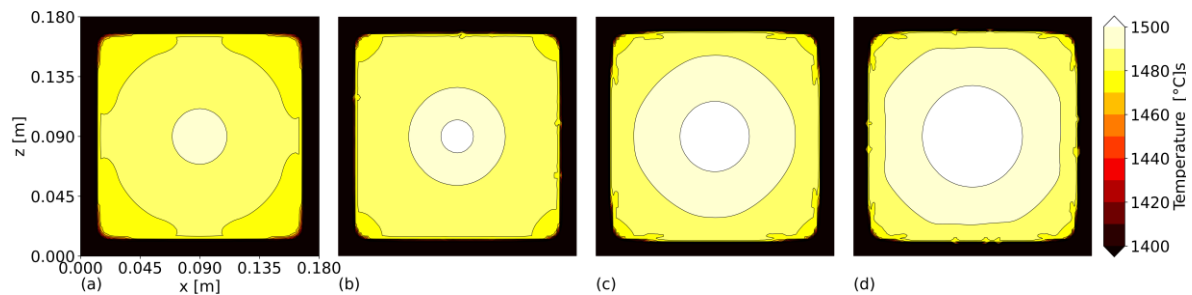


Figure 6. Comparison of temperature fields for different casting temperatures: a) 1505°C , b) 1515°C , c) 1525°C , and d) 1535°C , for a horizontal cross-section at 0.19 m , casting velocity 1.6 m/min and SEN depth 0.12 m .

The velocity field at horizontal cross-section $y = 0.19\text{ m}$ is presented next. Figure 7 shows velocity magnitude fields for different casting temperatures. Higher casting temperatures result in marginally higher velocities, which can be visible in the centre of the billet. At the boundary, velocities are constant and equal to casting velocity.

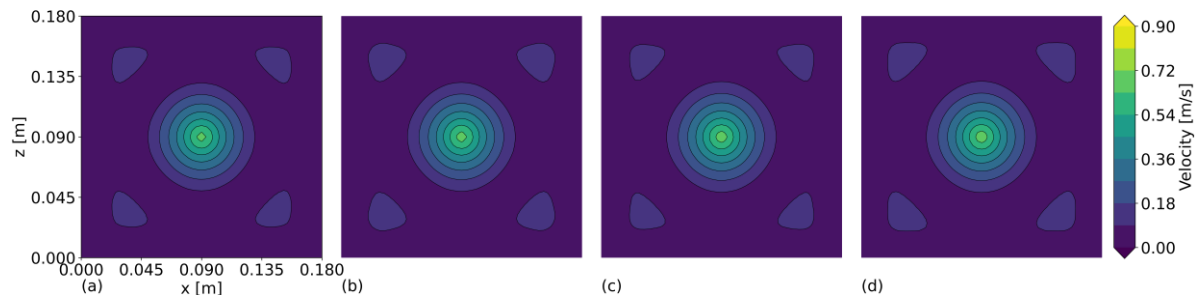


Figure 7. Comparison of velocity magnitude fields for different casting temperatures: a) 1505°C , b) 1515°C , c) 1525°C , and d) 1535°C , for a horizontal cross-section at 0.19 m , casting velocity 1.6 m/min and SEN depth 0.12 m .

The horizontal cross-section at $y = 0.19$ m and $z = 0.09$ m of velocity magnitude is shown in figure 8. The effect of casting temperature on velocity is negligible. We can observe small increase in the velocity with increasing casting temperature, however the differences are very small. A more pronounced effect can be seen when changing the casting velocity and SEN depth. The increase in SEN depth has similar effect as the increase in casting velocity, both of which result in slight increase of velocity magnitude in the centre of the billet.

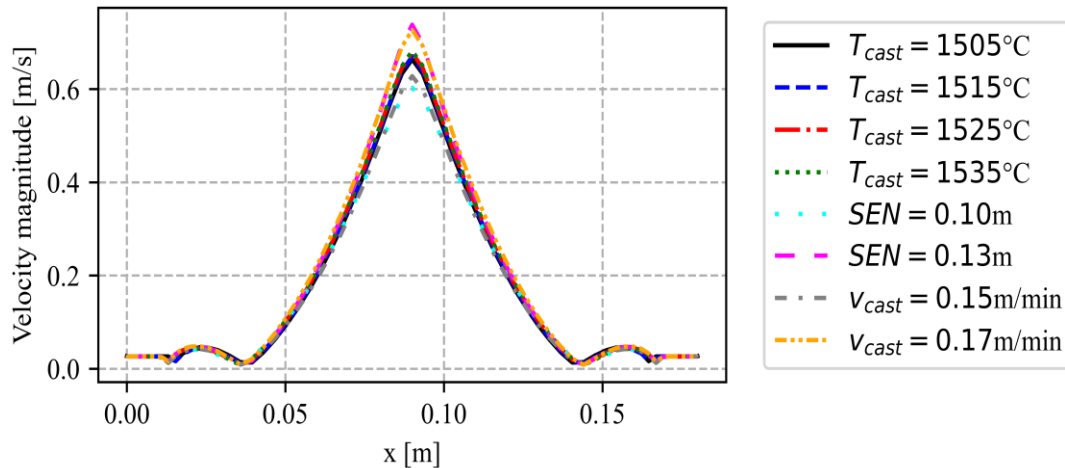


Figure 8. Comparison of velocity magnitude cross-sections for different casting temperatures, velocities and SEN depths.

Temperature cross-sections at $y = 0.19$ m and $z = 0.09$ m are presented in figure 9. Lower casting temperatures result in lower overall temperature in the central part of the billet. The change in central temperature at this cross-section due to the change in casting velocity is small. Bigger differences can be observed due to the change in the SEN depth.

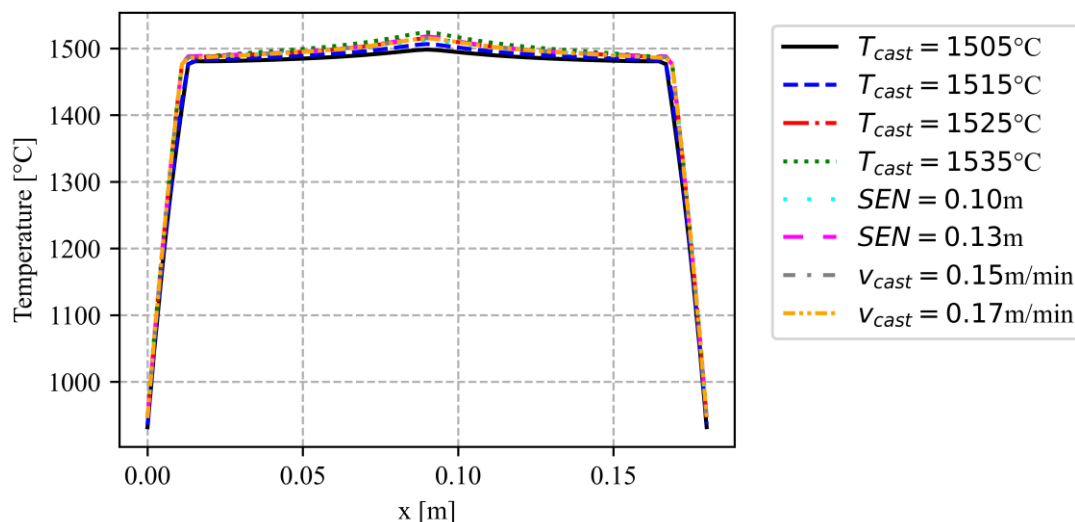


Figure 9. Comparison of temperature cross-sections for different casting temperatures, velocities and SEN depths.

This parametric study of our numerical model shows that the increase or decrease in the casting temperature has a more significant effect on the final solidification than the changes in the casting velocity or SEN depth.

6. Conclusions

The present study presents the macrosegregation in a 3D continuous casting mould solved with LRBFCM. The numerical example is evaluated for the Low-Re k-epsilon turbulence model. The results, calculated on 7-noded local subdomains with MQ RBFs, show a successful application of the RANS model for predicting macrosegregation in the 3D example of the CC of steel. Although lower casting temperatures result in a more homogenous concentration, slightly higher casting temperatures are used in real-life casting due to technological difficulties. The simulations will be compared with 3D LES model in the perspective paper [19].

Acknowledgements

This work was funded by the Slovenian Research Agency (ARRS) and Štore-Steel company in the framework of applied research project L2-3173 Advanced Simulation and Optimization of the Entire Process Route for Production of Topmost Steels, and program P2-0162 Multiphase Systems.

References

- [1] Vakhrushev A, Wu M, Ludwig A, Tang Y, Hackl G and Nitzl G 2012 *IOP Conf. Ser. Mater. Sci. Eng.* **33**
- [2] Aboutalebi M R, Hasan M and Guthrie R I L 1995 *Metall. Mater. Trans. B* **26** 731–44
- [3] Schneider M C and Beckermann C 1995 *Metall. Mater. Trans. A* **26** 2373–88
- [4] Zhang H, Nagaumi H, Zuo Y and Cui J 2007 *Mater. Sci. Eng. A* **448** 189–203
- [5] Gu J P P and Beckermann C 1999 *Metall. Mater. Trans. A Phys. Metall. Mater. Sci.* **30** 1357–66
- [6] Wu M, Ludwig A and Kharicha A 2019 *Metals*. **9**
- [7] Bozzini B, Antonetti L, Boniardi M, Serra M and Fanigliulo A 2002 *Int. J. Comput. Appl. Technol.* **15** 186–94
- [8] Mramor K, Vertnik R and Šarler B 2014 *3rd International Conference on Computational Methods for Thermal Problems, ThermaComp 2014* pp 283–6
- [9] Šarler B, Vertnik R and Mramor K 2012 *IOP Conf. Ser. Mater. Sci. Eng.* **33**
- [10] Vertnik R, Mramor K and Šarler B 2019 *Eng. Anal. Bound. Elem.* **104** 347–63
- [11] Vertnik R and Šarler B 2016 *IOP Conf. Ser. Mater. Sci. Eng.* **117**
- [12] Šarler B and Vertnik R 2006 *Comput. Math. with Appl.* **51** 1269–82
- [13] Bredberg J 2001 *On Two-equation Eddy Viscosity Models* (Goteborg)
- [14] Launder B 1974 *Int. Commun. Heat Mass Transf.* **1** 131–7
- [15] Steffen J R C 1993 *29th AIAA Joint Propulsion Conference and Exhibit* pp 1–13
- [16] Lilly D K 1966 *Natl. Cent. Atmos. Res.* **123**
- [17] Abe K, Kondoh T and Nagano Y 1995 *Int. J. Heat Mass Transf.* **38** 1467–81
- [18] Vertnik R and Šarler B 2014 *Eng. Anal. Bound. Elem.* **45** 45–61
- [19] Mramor K, Vertnik R and Šarler B 2022 *Metals (Basel)*. **12** 1–19